AGU PUBLICATIONS

Geophysical Research Letters

RESEARCH LETTER

10.1002/2015GL066275

Key Points:

- Albedo and cloud fraction are extremely well correlated over global ocean
- Models show too large spread in albedo for a given cloud fraction
- Present-day aerosols explain higher albedos for a given cloud fraction

Supporting Information:

- Figures S1–S3 and Table S1
- Figure S1
- Figure S2
- Figure S3

Correspondence to:
A. Engström,
anders@slb.nu

Citation:
Engström, A., F. A.-M. Bender, R. J. Charlson, and R. Wood (2015), The nonlinear relationship between albedo and cloud fraction on near-global, monthly mean scale in observations and in the CMIP5 model ensemble, *Geophys. Res. Lett.*, *42*, doi:10.1002/2015GL066275.

Received 21 SEP 2015
Accepted 27 OCT 2015
Accepted article online 4 NOV 2015

The nonlinear relationship between albedo and cloud fraction on near-global, monthly mean scale in observations and in the CMIP5 model ensemble

A. Engström[1], F. A.-M. Bender[1], R. J. Charlson[2], and R. Wood[2]

[1]Department of Meteorology and Bolin Centre for Climate Research, Stockholm University, Stockholm, Sweden,
[2]Department of Atmospheric Sciences, University of Washington, Seattle, Washington, USA

Abstract We study the relation between monthly mean albedo and cloud fraction over ocean, 60°S–60°N. Satellite observations indicate that these clouds all fall on the same near-exponential curve, with a monotonic distribution over the ranges of cloud fractions and albedo. Using these observational data as a reference, we examine the degree to which 26 climate models capture this feature of the near-global marine cloud population. Models show a general increase in albedo with increasing cloud fraction, but none of them display a relation that is as well defined as that characterizing the observations. Models typically display larger albedo variability at a given cloud fraction, larger sensitivity in albedo to changes in cloud fraction, and lower cloud fractions. Several models also show branched distributions, contrasting with the smooth observational relation. In the models the present-day cloud scenes are more reflective than the preindustrial, demonstrating the simulated impact of anthropogenic aerosols on planetary albedo.

1. Introduction

Clouds significantly alter the planetary albedo, approximately doubling the amount of reflected shortwave radiation on global mean scale [e.g., *Ramanathan et al.*, 1989; *Harrison et al.*, 1990]. The reflectivity of clouds and cloud-covered areas, and how they may change in the future due to increasing surface temperature (cloud feedback), are key to the understanding of present climate and climate change [*Bony and Dufresne*, 2005; *Webb et al.*, 2006; *Medeiros et al.*, 2008]. Previous studies have indicated that the scene albedo is strongly dependent on the cloud fraction, both on a global scale [*Loeb et al.*, 2007] and also more specifically for subtropical warm clouds [*George and Wood*, 2010].

Bender et al. [2011] have shown that for subtropical marine stratocumulus clouds in selected locations, the albedo is near-linearly dependent on cloud fraction, on the monthly mean scale. This means that individual clouds have sufficiently similar properties for the fractional area covered by clouds to be the primary determinant of the reflectivity. It has also been shown that state-of-the-art climate models capture this relationship quite well and that there has been an improvement in the representation of the radiative properties of these clouds, from the CMIP3 to the CMIP5 models (Coupled Model Intercomparison Project, phases 3 and 5) [*Engström et al.*, 2014]. At the same time most models do not exhibit a sufficiently high cloud fraction on the monthly mean scale, and have higher reflectivity than observations, which has been referred to as the "too few, too bright" problem, specifically of clouds in the tropics, in GCMs, previously identified and discussed by, e.g., *Nam et al.* [2012].

In this study, we take the analysis of *Bender et al.* [2011] and *Engström et al.* [2014] a step farther, no longer limiting the analysis to the cloud-wise relatively homogeneous stratocumulus regions. Although the relevance of these specific cloud regions for the radiation budget and climate has previously been demonstrated [e.g., *Ockert-Bell and Hartmann*, 1992; *Wood*, 2012], we here extend the analysis to include all marine cloud scenes between 60°S and 60°N. As in *Bender et al.* [2011], continental areas are excluded, to limit the influence of variable and high surface albedos on satellite albedo retrievals.

The relationship between albedo and cloud fraction has previously been presented in a similar way, using global scale daily mean data for one specific month, obtained from satellite observations and three individual climate models [*Webb et al.*, 2001].

This analysis suggested a weakly nonlinear relationship between albedo and cloud fraction, with an increasing scatter in albedo with increasing cloud fraction. However, daily output is not available for the majority of the CMIP5 models on global scale, and we here focus on the climatologically relevant monthly mean time scale, allowing for comparison with a large number of climate models and also making the analysis directly comparable to that of *Bender et al.* [2011] and *Engström et al.* [2014]. We study the near-global monthly mean scale relation between cloud fraction and albedo in satellite observations, compare it with the results of an ensemble of climate models, and also investigate the change in the model-simulated relation resulting from the application of anthropogenic forcing.

2. Methods and Data

We analyze monthly mean all-sky albedo and cloud fraction derived from the CERES (Clouds and the Earth's Radiant Energy System) [*Wielicki et al.*, 1996] and MODIS (MODerate resolution Imaging Spectroradiometer) [*Minnis et al.*, 2011] instruments on the polar orbiting satellites Aqua and Terra. Terra and Aqua cross the equator at 10:30 and 13:30 local time, respectively, and we study the mean values constructed from these two overpasses, capturing a fraction of the full day that the climate model output is averaged over. The period of study spans from July 2002 to July 2014, and the data, which are part of the Single Satellite Footprint collection (SSF1-deg Edition 2.7), are analyzed on a 1° × 1° resolution over the global ocean between 60°S and 60°N.

Monthly mean simulated fields of top-of-atmosphere albedo and total cloud fraction from 26 models and model versions participating in the Climate Model Intercomparison Project, phase 5 (CMIP5) [*Taylor et al.*, 1996] are also analyzed. We make use of two different sets of simulations, corresponding to present-day (PD) conditions and preindustrial (PI) conditions, respectively, to study the effect of anthropogenic forcing. The models, their resolutions, and the responsible institutions are listed in Table S1 in the supporting information. We use 25 years of model output for each model and in each set of simulations, using emissions representative of conditions before 1850 for the PI simulations and for the period 1980–2004 for the PD simulations.

In our analysis we study two-dimensional histograms of monthly mean cloud fraction and albedo. The data are normalized with respect to the total number of values of albedo and cloud fraction in each data set, and the histograms represent the frequency of occurrence of specific combinations of albedo and cloud fraction values.

The analysis is based on the variable cloud fraction, although we note that its exact definition may differ between models and between models and satellite observations. The estimation of total cloud fraction is associated with uncertainty, in the sense that its quantification based on one instrument or model may be different from that acquired by another. Still, cloud fraction is readily available as a product from observations and models and because of its control on a key climatic variable (albedo) it becomes important to study in a diagnostic sense. Differences in definitions and detection algorithms between satellite retrievals and model simulations, for instance, due to different assumptions of the threshold for what constitutes a cloud, different vertical cloud overlap algorithms, and different temporal sampling, may lead to discrepancies. Satellite simulators, which account for some of these differences, have been implemented in several of the CMIP5 models, but unfortunately no simulator data for the MODIS instrument, on which the present analysis relies, is available in the CMIP5 database. Therefore, we choose to analyze cloud fraction as it is given in the models and data sets while keeping these limitations in mind.

Lastly, we note that the satellite data captures only a fraction of the full day that the climate model output is averaged over. We find that contrasting the sampling times of Aqua and Terra does not affect the results, but the lack of diurnal sampling may still lead to an underestimation of the variability in albedo in observations. We also note that the albedo is more sensitive to differences in optical properties of clouds and differences in cloud fraction at high solar zenith angle, contributing to a nonlinear relation between albedo and cloud fraction.

3. Results

3.1. Observed Relationship Between Albedo and Cloud Fraction

Figure 1 shows the distribution of monthly mean total albedo from CERES and cloud fraction from MODIS, for all points over ocean between 60°S and 60°N. Noticeably, all observed cloud scenes fit on the same curve, and most of the variability in albedo on this spatiotemporal scale appears to be controlled by the mean cloud fraction. The small range in albedo for each given cloud fraction indicates second-order variability in cloud optical

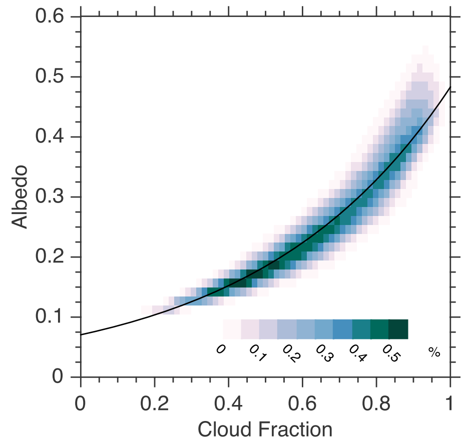

Figure 1. The relationship between 1° × 1° monthly mean albedo and cloud fraction for all ocean regions between 60°S and 60°N, with cloud fraction and albedo from MODIS and CERES, respectively. The color scale represent the frequency of occurrence in per cent for each combination of cloud fraction and albedo values. The black line represents the exponential least squares fit to the data.

thickness, and we note that this variability is significantly smaller in the monthly averaged data presented here than in daily data, as displayed by *Webb et al.* [2001]. The correlation between cloud fraction and the logarithm of albedo is 0.94, indicating a near-exponential dependence of albedo on cloud fraction. We also note that the frequency distribution of the observations in albedo-cloud fraction space is more or less continuous; i.e., there is no specific combination of albedo and cloud fraction which is dominatingly preferred, although the frequency of occurrence of low values of cloud fraction and albedo is slightly increased compared with other values. These cases typically correspond to subtropical latitude bands, as can be seen from Figure S1.

Following the exponential relationship, the slope of the observed curve varies with cloud fraction. As cloud fraction increases, the slope becomes steeper, indicating that the albedo sensitivity to changes in cloud fraction is greater, or, in other words, that there may be a positive correlation between cloud fraction and cloud optical depth. This supports previous findings from other satellite observations (ERBE and ISCCP) on daily time scale [*Webb et al.*, 2001]. However, the increasing albedo sensitivity with increasing cloud fraction may also partly be an effect of latitudinal dependence of albedo, i.e., that the albedo of a given cloud is higher at high solar zenith angle. Comparatively, high solar zenith angles coinciding with regions where there is typically more clouds (i.e., midlatitudes) would also yield a correlation between cloud fraction and albedo sensitivity.

Figure 1 further indicates that the spread in albedo for a given cloud fraction is dependent on cloud fraction; at higher cloud fraction the variability is larger. The variability is also larger at larger cloud fractions in a relative sense (i.e., when divided by the mean albedo in each cloud fraction range), indicating that the increase in spread is not only an effect of a higher mean albedo at higher cloud fraction (not explicitly shown). This points to the importance of variability in the reflection of sunlight by clouds in driving the variability in total albedo.

3.2. Relationship Between Albedo and Cloud Fraction in the CMIP5 Model Ensemble

Figure 2 shows the relationship between albedo and cloud fraction in each of the 26 CMIP5 models for present-day conditions. The CMIP5 models are able to qualitatively reproduce the exponential relationship between cloud fraction and cloud albedo. However, compared to the satellite data, a much more diversified picture of the relationship emerges. There is a substantial intermodel disagreement in the relationship between albedo and cloud fraction, and also, with the exception of a few models, a strong disagreement with the satellite observations. Generally, the CMIP5 models display a less well-defined frequency distribution in albedo-cloud fraction space with a larger range of albedo values occurring for any given cloud fraction. The disagreement may be caused by errors in models as well as observational data, but given the intermodel differences and the agreement between different observational data sets for more limited geographical regions [*Bender et al.*, 2011], we take the observations as a reference that the models should ideally agree with.

All models tend to overestimate the total albedo for any given cloud fraction, compared to observations and typically show that cloud fraction distributions shifted to lower values, indicating that the "too few, too bright" problem previously demonstrated for low warm tropical clouds [*Nam et al.*, 2012], is applicable on larger scale. The models also tend to display a higher sensitivity of albedo to changes in cloud fraction as seen from the generally larger increase in albedo with increasing cloud fraction. Assuming that potential biases in clear-sky effects are negligible, this points at clouds in the models being optically thicker than those observed.

Several models (e.g., the BCC-CSM1-1, GFDL-CM3, INMCM4, the IPSL and MIROC families of models, and the MPI-EMS-LR) display branched, binary or ternary distributions, in contrast with the unified smooth distribution in the satellite data. This indicates the presence of different categories of clouds that occur in similar

10.1002/2015GL066275

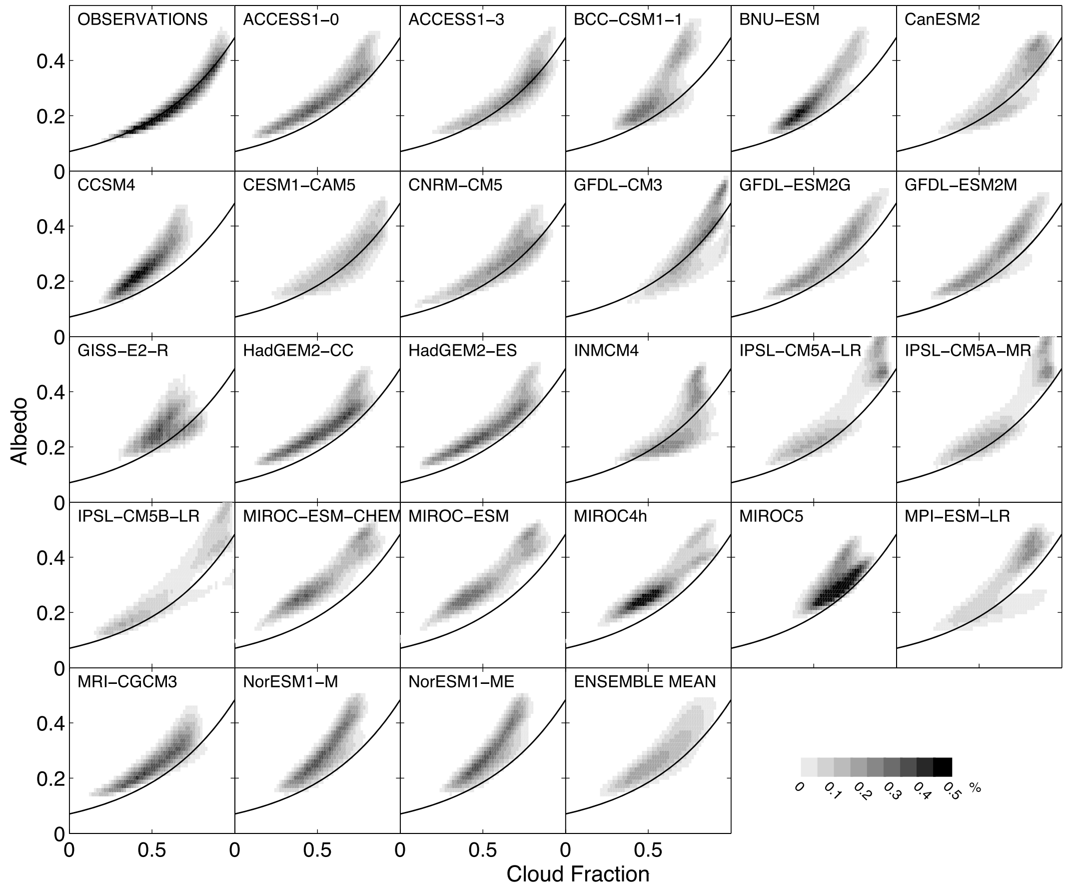

Figure 2. The relationship between albedo and cloud fraction for all ocean regions between 60°S and 60°N displayed as two-dimensional histograms for all 26 participating CMIP5 models. The gray scale represent the frequency of occurrence in percent for each combination of cloud fraction and albedo values. The black lines in each panel represent the exponential least squares fit to the satellite observations shown in Figure 1 and reproduced in the top left panel. The bottom right panel shows the model ensemble mean. Observational monthly mean data are averaged over 1° × 1° and model monthly mean data are analyzed on grids corresponding to the horizontal resolution of each model, see Table S1.

amount (cloud fraction) but are related to different total albedo, i.e., have different optical depth. According to Figure S1 it is typically extensive low-latitude clouds with low optical depth that create a separate branch in albedo-cloud fraction space in these models.

Several models (e.g., ACCESS1-3, BCC-CSM1-1, BNU-ESM, INMCM-4, the IPSL models, the MIROC models, and the MPI-ESM-LR), much more than the observations, show preferred states of certain combinations of albedo and cloud fraction. The presence of these more or less distinct maxima indicates higher frequency of occurrence of cloud scenes with similar optical properties and cloud fractions, i.e., too little regional and temporal variation in cloud fraction and albedo. Based on the latitudinal distribution shown in Figure S1, this is also equivalent to clouds being too concentrated at distinct latitudes. The remaining models have frequency distributions more similar to the observations, in this respect.

The ACCESS1-0 and HadGEM2 models do show a relatively well-defined (compared with the remaining models) continuous exponential relationship although they display an additional curve branching to higher albedos from the rest of the data at high cloud fractions. These two models share the same atmospheric physical parameterizations as they both use the Met Office Unified Model as their atmospheric component.

The model diversity in albedo sensitivity to increasing cloud fraction speaks against the latitudinal dependence of albedo explaining this relation, and thereby the exponential shape found in the observations, as an albedo dependence on solar zenith angle should be similar across models.

10.1002/2015GL066275

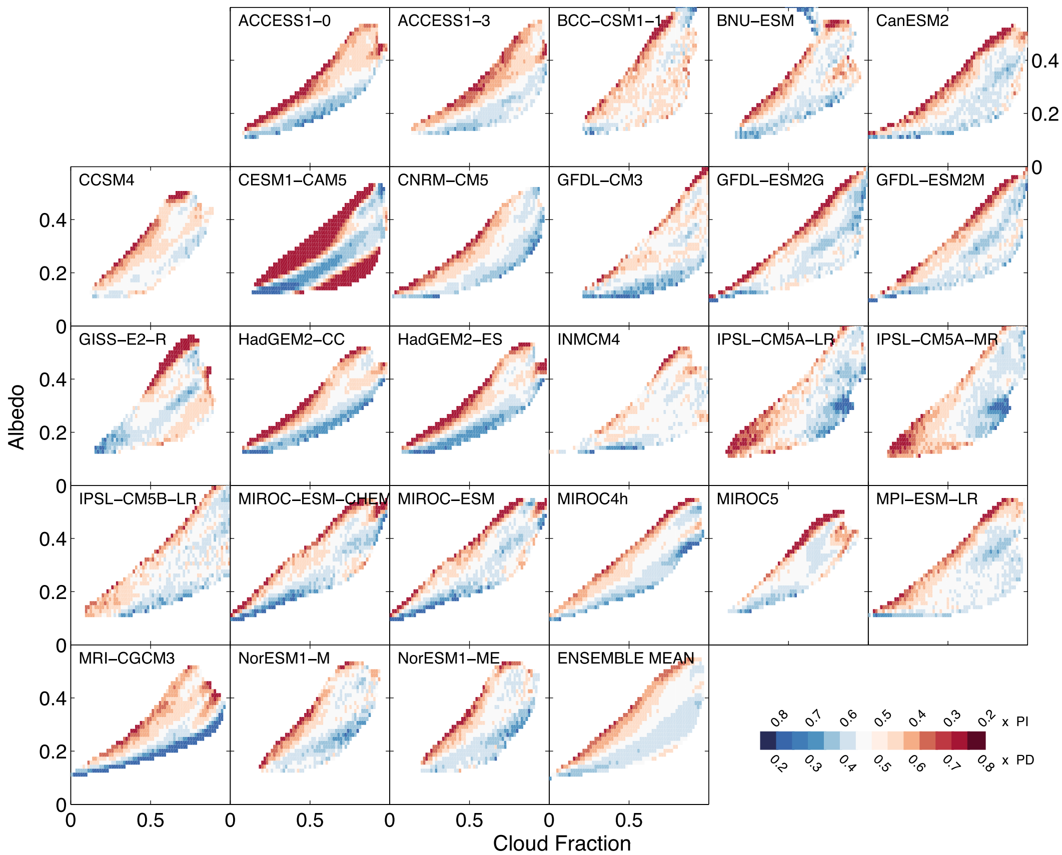

Figure 3. The difference in the distribution of values in albedo-cloud fraction space between the PI and PD simulations. Colors represent the fraction of data in each grid square in albedo-cloud fraction space belonging to the PI (blue) and the PD simulations (red), respectively. The bottom right panel shows the corresponding shift in the model ensemble mean.

3.3. Change in the Relationship Between Cloud Fraction and Albedo Between Preindustrial and Present-Day Conditions

In the climate models it is possible to study the potential change in the relationship between albedo and cloud fraction related to changes in forcing from PI to PD conditions. In Figure 3 the albedo and cloud fraction distributions over the 60°S to 60°N ocean are shown simultaneously for the two different sets of model simulations. The color coding indicates the fraction of points belonging to PI (blue) and PD (red) simulations respectively, following *Engström et al.* [2014]. Additionally, in Figures S2 and S3 one-dimensional histograms are shown for the difference between PD and PI simulations for cloud fraction and albedo, separately, to help determine if the gradient shown in Figure 3 is mainly caused by differences in cloud fraction or albedo.

The model diversity is large, but in general, there is indication of PD simulations typically having higher albedos for a given cloud fraction which is represented by the color gradient in albedo for any given cloud fraction. For models that display a binary or ternary distribution (in Figure 2) we note that this shift appears to be acting for each of the separate branches, e.g., in the ACCESS1-3, CNRM-CM5, GFDL-CM3, HadGEM2, and MRI-CGCM3 models.

The IPSL family of models, and to some extent the MPI-ESM-LR model, show a shift toward a lower cloud fraction and a lower albedo in the PD simulations (see Figures S2 and S3). For the NorESM1 family of models, and the CNRM-CM5 model, the color gradient shown in Figure 3 appears to be caused mainly by a shift in cloud fraction toward lower values under PD conditions (see Figures S2 and S3).

The CESM1-CAM5 and GISS-E2-R models show a different behavior of low-latitude cloud scenes compared to the other models. Apart from an overall shift to higher albedos for any given cloud fraction, both of these models also display a clear shift of low-latitude cloud scenes to higher cloud fraction values such that the

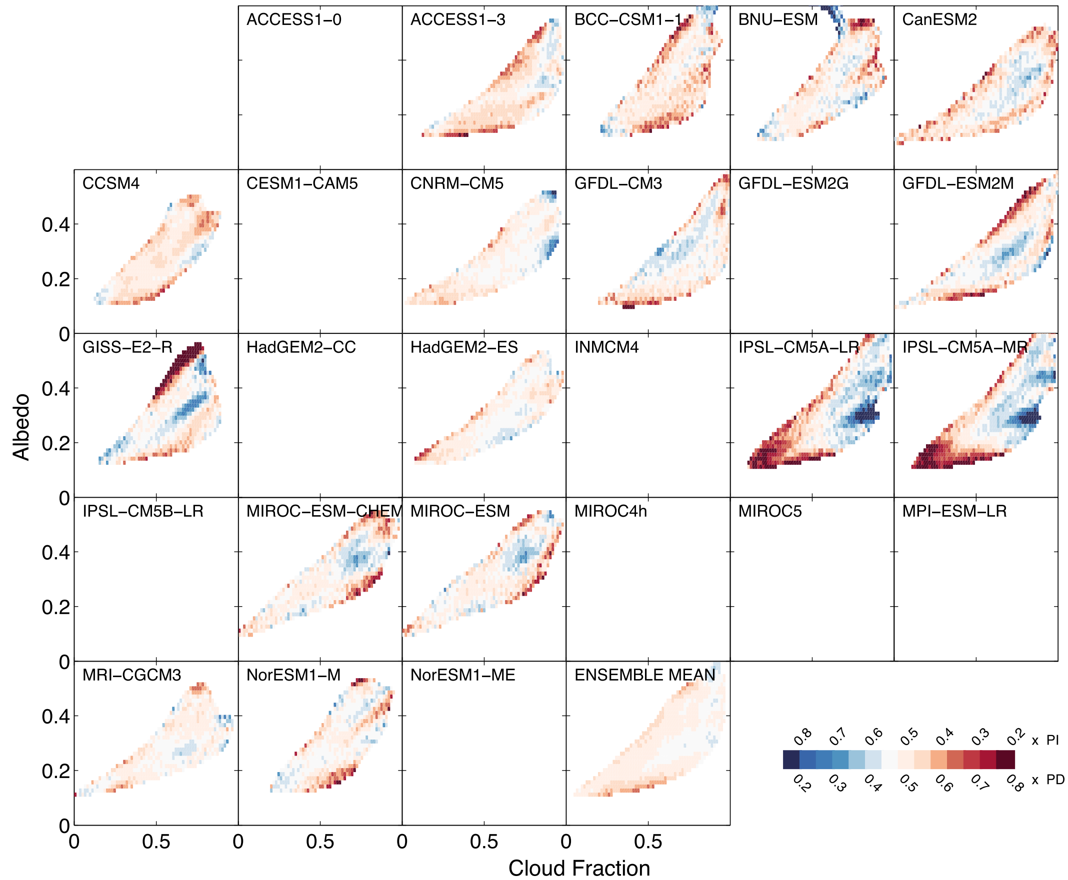

Figure 4. The difference in the distribution of values in albedo-cloud fraction space between simulations with increases in greenhouse gases only, from PI to PD levels. Colors represent the fraction of data in each grid square in albedo-cloud fraction space belonging to the PI (blue) and the PD (red) greenhouse gas level simulations, respectively. The bottom right panel shows the corresponding shift in the model ensemble mean.

frequency of occurrence of scenes with an extensive cloud cover of optically thin clouds is increased in PD conditions.

The ensemble mean of the shift in all models displays a uniform and clear increase in the scene albedo for any given cloud fraction. At low cloud fraction, this may be indicative of the increased scattering of sunlight by aerosols in PD conditions whereas for higher cloud fraction, it is more likely to be related to differences in the cloud optical thickness of clouds, caused either by differences in the amount of condensed water or in differences in the size distribution of cloud particles possibly caused by aerosol-cloud interactions.

In the PD simulations, both aerosols and greenhouse gases are increased to represent present-day conditions. However, several model centers also provide simulations with only increased levels of greenhouse gases, making it possible to separate effects of aerosols on clouds from cloud feedbacks to the greenhouse gas induced warming. Model simulations with increased levels of greenhouse gases only do not typically show higher albedos for a given cloud fraction. Instead, less organized shifts to both lower and higher albedos, as well as lower and higher cloud fractions appear to take place, see Figure 4. Some signals observed in Figure 3 do seem to originate from the increased levels of greenhouse gases, for instance, the strong increase in albedo for the GISS-E2-R model at high cloud fractions and the shift to lower albedo and lower cloud fraction for the IPSL-CM5A-LR and IPSL-CM5A-MR models. The ensemble mean of the models that provide simulations with only increased levels of greenhouse gases differs significantly from that of both increased levels of greenhouse gases and aerosols, indicating that it is mainly the difference in atmospheric aerosol concentrations in models that creates the patterns seen in Figure 3.

4. Discussion and Conclusions

The relation between albedo and cloud fraction over the near-global (60°S–60°N) ocean, as deduced from satellite observations and from an ensemble of current generation climate models, is investigated. In the satellite observations, a near-exponential increase in albedo with cloud fraction in the monthly mean is seen, and *all* the marine cloud scenes studied can be referred to the same curve, frequency of occurrence of individual albedo, and cloud fraction combinations evenly distributed. In the CMIP5 ensemble, on the other hand, there are model-specific examples of branched distributions, binary and ternary, as well as apparent preferred states of cloud fraction and albedo, with greater representation than others.

The models typically display a too high sensitivity of albedo to differences in cloud fraction, indicating too large optical thickness of the clouds, and too large spread in albedo for any given cloud fraction, indicating too large variability in cloud optical thickness. The same kind of enhanced variability in models has been found for subtropical stratocumulus clouds [*Engström et al.*, 2014], and reasons for this discrepancy between models and observations still require further investigation. Further, many models do not exhibit high enough cloud fraction on the monthly mean scale. There are, however, significant intermodel differences, and the mean of the model ensemble shows a closer resemblance to the observations than do the individual models.

In addition to serving as a way to test model ability to simulate observed current cloud properties, the presented analysis also holds powerful diagnostic information regarding the sensitivity of models to forced changes in cloud fraction. For example, a model displaying a stronger increase in albedo with increasing cloud fraction may be expected to show a stronger sensitivity to modeled differences in cloud fraction in predictions of future climate compared to a model that displays an albedo that is relatively insensitive to cloud fraction changes. In fact, if the slope of the linear fit between cloud fraction and the logarithm of albedo is taken as a measure of a model's sensitivity to cloud fraction changes, this measure is weakly correlated to both cloud radiative effects and net radiative effects as reported for a subset of the CMIP5 models reported in *Tomassini et al.* [2013] and *Andrews et al.* [2012] Additionally, the separate branch of the relationship between albedo and cloud fraction for low-latitude tropical and subtropical clouds that is apparent in several models, typically shows a substantially smaller sensitivity to changes in cloud fraction compared to other regions and cloud types. It is possible that this makes these models less sensitive to differences in the extent and optical properties of tropical marine clouds, features that have previously been discussed as being the primary components of uncertainty related to cloud feedbacks [*Bony and Dufresne*, 2005].

Comparing simulations representing preindustrial and present-day conditions, we find that the forced simulations, in general, display higher albedo values for a given cloud fraction, indicating that cloud scenes in present-day climate are brighter than those in preindustrial climate. There is, however, some diversity among the models in this relation, and while some models indicate that such a brightening is most prominent at low cloud fractions of optically thin clouds, others indicate that it rather takes place at higher cloud fractions of optically thick clouds, and in a few cases, a reversal of the relationship is seen, indicating a darkening for certain cloud scenes. By studying simulations with only increased levels of greenhouse gases, we also find that these shifts are mainly caused by differences in the atmospheric aerosol loading between present-day and preindustrial conditions and not because of differences in greenhouse gases.

While intermodel differences in the relationship between albedo and cloud fraction may partially be explained by differences in the definition of cloud fraction, the comparison between individual models and observations is still a useful diagnostic.

To the extent that the observations are representative of the true relationship between albedo and cloud fraction, also supported by independent observations using other satellite instruments [*Webb et al.*, 2001; *Bender et al.*, 2011], modelers should strive to replicate the observed relationship as the radiative effect of differences in cloud optical properties in a model depends greatly on the frequency distribution of cloud scenes in albedo-cloud fraction space. The analysis presented here may be used to facilitate such efforts of model improvement. While the diagnostic presented here is based on monthly averaged data, the same method may also be used for evaluation of model output of higher temporal frequency, using satellite data down to daily time scale.

Acknowledgments
We acknowledge the World Climate Research Programme's Working Group on Coupled Modeling, which is responsible for CMIP, and we thank the climate modeling groups (listed in Table S1 in the supporting information of this paper) for producing and making available their model output. For CMIP the U.S. Department of Energy's Program for Climate Model Diagnosis and Intercomparison provides coordinating support and led development of software infrastructure in partnership with the Global Organization for Earth System Science Portals. We also thank the NASA Langley Atmospheric Science Data Center, for satellite data distribution.

References

Andrews, T., J. M. Gregory, M. J. Webb, and K. E. Taylor (2012), Forcing, feedbacks and climate sensitivity in CMIP5 coupled atmosphere-ocean climate models, *Geophys. Res. Lett.*, *39*, L09712, doi:10.1029/2012GL051607.

Bender, F. A.-M., R. J. Charlson, A. M.-L. Ekman, and L. Leahy (2011), Quantification of monthly mean regional scale albedo of marine stratiform clouds in satellite observations and GCMs, *J. Appl. Meteorol. Clim.*, *50*, 2139–2148.

Engström, A., F. A. -M. Bender, and J. Karlsson (2014), Improved representation of marine stratocumulus cloud shortwave radiative properties in the CMIP5 climate models, *J. Clim.*, *27*, 6175–6188.

Bony, S., and J.-L. Dufresne (2005), Marine boundary layer clouds at the heart of tropical cloud feedback uncertainties in climate models, *Geophys. Res. Lett.*, *32*, L20806, doi:10.1029/2005GL023851.

George, R. C., and R. Wood (2010), Subseasonal variability of low cloud radiative properties over the southeast Pacific Ocean, *Atmos. Chem. Phys.*, *10*, 4047–4063.

Harrison, E. F., et al. (1990), Seasonal variation of cloud radiative forcing derived from the Earth Radiation Budget Experiment, *J. Geophys. Res.*, *95*, 18,687–18,703.

Loeb, N. G., B. A. Wielicki, F. G. Rose, and D. R. Doelling (2007), Variability in global top-of-atmosphere shortwave radiation between 2000 and 2005, *Geophys. Res. Lett.*, *34*, L03704, doi:10.1029/2006GL028196.

Medeiros, B., B. Stevens, I. M. Held, M. Zhao, D. L. Williamson, J. G. Olson, and C. S. Bretherton (2008), Aquaplanets, climate sensitivity, and low clouds, *J. Clim.*, *21*, 4974–4991.

Minnis, P., et al. (2011), CERES edition-2 cloud property retrievals using TRMM VIRS and Terra and Aqua MODIS data, Part I: Algorithms, *IEEE Trans. Geosci. Remote Sens.*, *49*, 4374–4400.

Nam, C., S. Bony, J.-L. Dufresne, and H. Chepfer (2012), The 'too few, too bright' tropical low-cloud problem in CMIP5 models, *Geophys. Res. Lett.*, *39*, L21801, doi:10.1029/2012GL053421.

Ockert-Bell, M. E., and D. L. Hartmann (1992), The effect of cloud type on the Earth's energy balance: Results for selected regions, *J. Clim.*, *5*, 1157–1171.

Ramanathan, V., R. D. Cess, E. F. Harrison, P. Minnis, B. R. Barkstrom, E. Ahmad, and D. Hartmann (1989), Cloud-radiative forcing and climate: Results from the Earth radiation budget experiment, *Science*, *56*, 67–63.

Taylor, K. E., R. J. Stouffer, and G. A. Meehl (1996), An overview of CMIP5 and the experiment design, *Bull. Am. Meteorol. Soc.*, *93*, 485–498.

Tomassini, L., O. Geoffroy, J.-L. Dufresne, A. Idelkadi, C. Cagnazzo, K. Block, T. Mauritsen, M. Giorgetta, and J. Quaas (2013), The respective roles of surface temperature driven feedbacks and tropospheric adjustment to CO_2 in CMIP5 transient climate simulations, *Clim. Dyn.*, *41*, 3103–3126.

Webb, M., C. Senior, S. Bony, and J. J. Morcrette (2001), Combining ERBE and ISCCP data to assess clouds in the Hadley Centre, ECMWF and LMD atmospheric climate models, *Clim. Dyn.*, *17*, 905–922.

Webb, M. J., et al. (2006), On the contribution of local feedback mechanisms to the range of climate sensitivity in two GCM ensembles, *Clim. Dyn.*, *27*, 17–38.

Wielicki, B. A., B. R. Barkstrom, E. F. Harrison, R. B. Lee III, G. L. Smith, and J. E. Cooper (1996), Clouds and the Earth's Radiant Energy System (CERES): An Earth observing system experiment, *Bull. Am. Meteorol. Soc.*, *77*, 853–868.

Wood, R. (2012), Stratocumulus clouds. Review, *Mon. Weather Rev.*, *140*, 2373–2423.